Chapter 12

Tracing Reversible Light-Induced Chromatin Binding with Near-infrared Fluorescent Proteins

Anne Rademacher, Fabian Erdel, Jorge Trojanowski, and Karsten Rippe

Abstract

Blue light-induced chromatin recruitment (BLInCR) is a versatile optogenetic tool to enrich effector proteins at specific loci within the nucleus using illumination in the 400–500 nm range. The resulting chromatin binding reaction is reversible on the time scale of minutes. BLInCR is advantageous over ligand-binding induced methods since it does not require a change of growth medium for the relatively slow depletion of the inducer from the nucleus. However, applying BLInCR for reversibility experiments is challenging because of the need to spectrally separate light-induced activation from visualization of the chromatin locus and effector and/or reader proteins by light microscopy. Here, we describe an improved BLInCR protocol for light-dependent association and dissociation of effectors using the near-infrared fluorescent protein iRFP713. Due to its spectral properties, iRFP713 can be detected separately from the red fluorescent protein mCherry. Thus, it becomes possible to trace two proteins labeled with iRFP713 and mCherry independently of the light activation reaction. This approach largely facilitates applications of the BLInCR system for experiments that test the reversibility, persistence, and memory of chromatin states.

Key words Optogenetics, Transcription activation, Automated microscopy, Image quantification, Chromatin binding

1 Introduction

Optogenetic proteins switch their conformation when illuminated with light of a certain wavelength range and revert to their original conformation in the absence of this trigger [1]. When exploiting the light-dependent reversibility—an inherent advantage of optogenetic systems—for microscopy studies, the repertoire of usable fluorescent protein tags is limited to excitation wavelengths outside the range that induces photoswitching. Two widely used blue light-induced photoswitches are the PHR domain from *Arabidopsis thaliana* [2, 3] and the LOV2 domain from *Avena sativa* [4, 5], which change their interaction properties in response to blue light. Fluorescently tagged proteins used in combination with these photoswitches need to be excited with green or longer wavelength

Dominik Niopek (ed.), *Photoswitching Proteins: Methods and Protocols*, Methods in Molecular Biology, vol. 2173,
https://doi.org/10.1007/978-1-0716-0755-8_12,

light to visualize them without inducing photoswitching [3, 6]. Thus, commonly used fluorescent proteins such as CFP, GFP or YFP are not suited. Red fluorescent proteins such as mCherry ($\lambda_{ex} = 587$ nm, $\lambda_{em} = 610$ nm) [7] are compatible with the excitation wavelength requirements. However, it is often desirable to monitor a second protein independently of the photoswitch trigger, for example, to determine the location of the chromatin locus of interest or to include a functional readout for the recruited effector. To address this issue, fluorescent proteins with near-infrared emission [8] such as iRFP713 ($\lambda_{ex} = 690$ nm, $\lambda_{em} = 713$ nm) [9] can be used (*see* **Note 1**). By sequential image acquisition on a confocal fluorescence microscope with $\lambda_{ex1} = 633$ nm and $\lambda_{ex2} = 561$ nm and appropriately selected detection windows, the iRFP713 and mCherry signals can be spectrally separated and recorded without inducing blue light-dependent photoswitching (Fig. 1).

BLInCR relies on the PHR domain that switches to a conformation that is permissive for interaction with CIBN when illuminated with blue light [10]. In this system, CIBN is fused to a nuclear protein that adopts a specific localization in the nucleus (e.g., reporter gene arrays, telomeres, nucleoli, PML nuclear bodies or the nuclear lamina). Blue-light illumination in the 400–500 nm range results in high local concentration of PHR-fused effector proteins at the target site. This approach was applied previously to dissect gene expression kinetics by fusing CIBN to TetR and PHR to the transcriptional activator VP16 or a nuclear localization signal (NLS, mock effector) [10]. A detailed protocol for this application can be found elsewhere [11]. The U2OS 2-6-3 cell line [12] was used for these experiments. It contains an array consisting of repetitive, promoter-proximal binding sites for LacI and TetR and a reporter cassette comprising a gene with MS2 loops that codes for peroxisome-targeted CFP (Fig. 2a). Previously, we used a GFP array marker to visualize the reporter array in this cell line. Since GFP-based imaging is incompatible with reversibility experiments, we recorded *z*-stacks of the mCherry-tagged effector to ensure that we capture the entire signal from the array [10]. Here, we provide a detailed protocol for recording effector and localizer fluorescence independently of the BLInCR blue light trigger via mCherry and iRFP713 fusions. This approach reduces the imaging time (and thereby photobleaching) and simplifies the image analysis (Fig. 2b, c). In addition, recruitment and reversibility can be characterized with the same constructs in the same cell. This is beneficial for rigorously resolving differences among individual cells during complex activation-deactivation patterns.

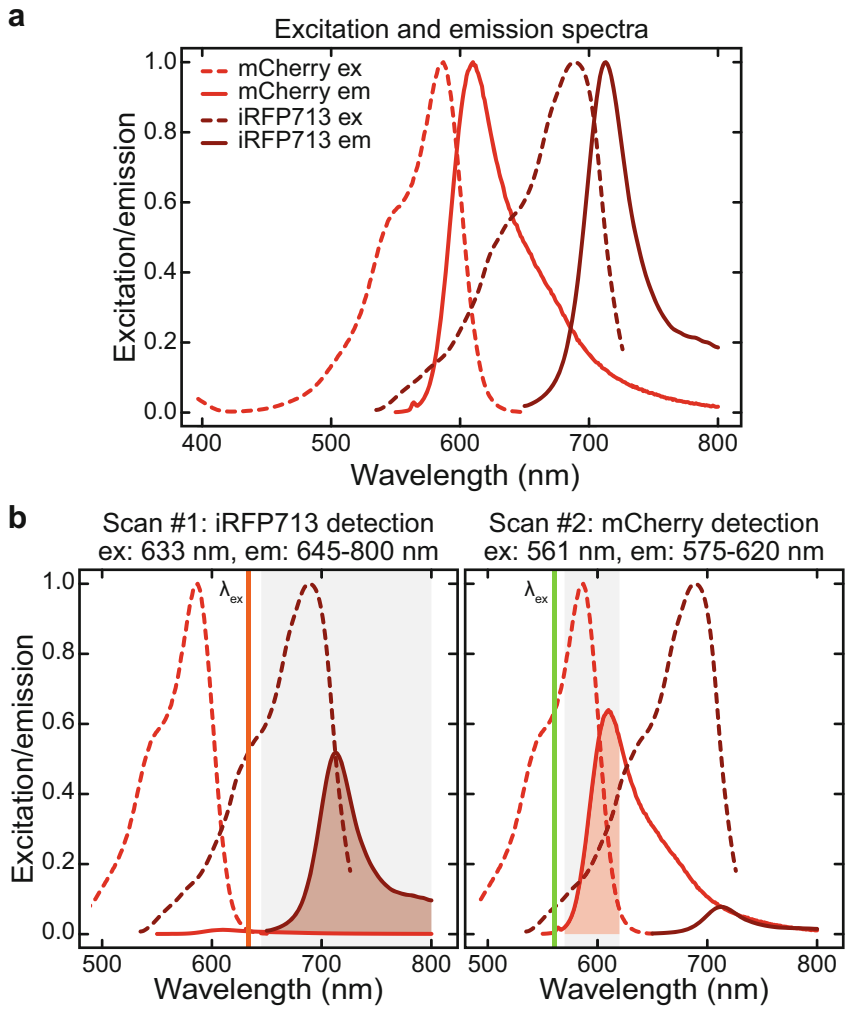

Fig. 1 Fluorescent proteins used for BLInCR reversibility experiments. (**a**) Excitation (dashed line) and emission (solid line) spectra of the red fluorescent protein mCherry and the near-infrared fluorescent protein iRFP713. The spectra are normalized to their respective maxima. (**b**) For the experiments described here, fluorescence is recorded in two sequential scans with the excitation wavelength (λ_{ex}) marked by a solid vertical line and the emission detection window marked by grey boxes. The emission spectra are scaled to the relative excitation at the excitation wavelength λ_{ex}. ex, excitation; em, emission

2 Materials

2.1 Cell Culture

1. Reporter cell line U2OS 2-6-3 [12] or other cell line containing repetitive arrays of *tet*O or *lac*O that can be bound by TetR or LacI, respectively (*see* **Note 2**).
2. Low glucose (1.0 g/L) DMEM without phenol red (ThermoFisher Scientific Inc., USA) supplemented with 10% tetracycline-free fetal bovine serum (FBS), 2 mM stable glutamine, 1× Penicillin/Streptomycin.

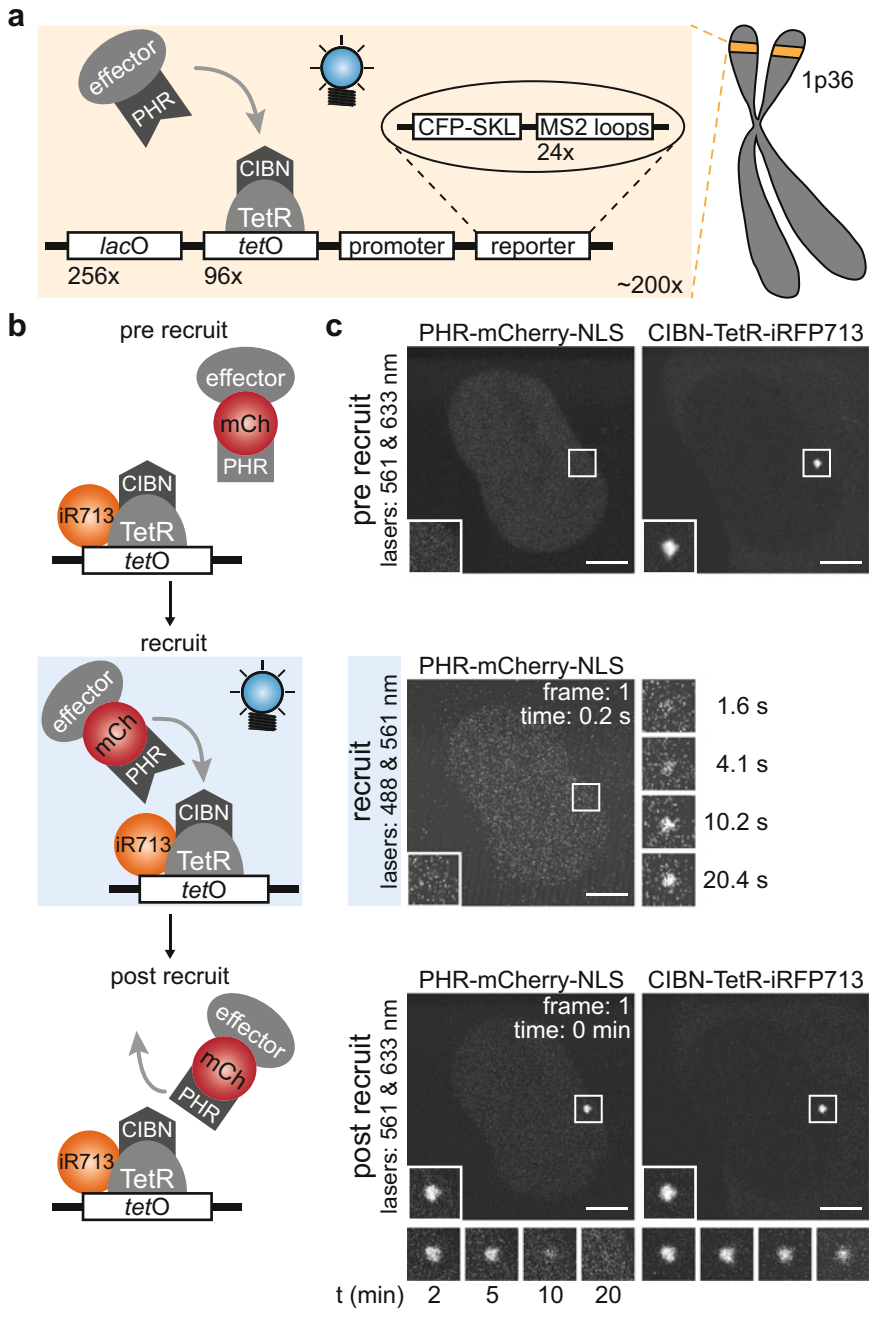

Fig. 2 Setup for BLInCR experiments with iRFP713. (**a**) The U2OS 2-6-3 cell line [12] contains promoter-proximal *tet*O and *lac*O arrays for TetR and LacI binding, respectively, that can be targeted by corresponding localizers fused to CIBN. In addition, it contains reporters for RNA (MS2) and protein (peroxisome-targeted CFP) readouts. (**b**) Schematic representation of pre recruit, recruit, and post recruit events for effector BLInCR to *tet*O arrays. The fluorophores can be visualized at every step independently of blue light-induced effector

3. Phosphate-buffered saline (PBS).
4. 0.05% trypsin/0.02% EDTA in PBS.
5. 8-well Lab-Tek chambers (ThermoFisher Scientific Inc.) or any other cell culture dish that is suitable for live cell microscopy (*see* **Note 3**).
6. Xtreme Gene 9 (Roche, Germany) or any other suitable transfection reagent (*see* **Note 4**) as well as transfection media, if needed (e.g., Opti-MEM for Xtreme Gene 9).
7. BLInCR constructs: CIBN-TetR-iRFP713 (localizer, *see* **Note 5**), PHR-mCherry-VP16 (effector, Addgene #103821), PHR-mCherry-NLS (mock effector, Addgene #103819) (*see* **Note 6**).
8. Nontransparent Styrofoam box (*see* **Note 7**).
9. Red flashlight (*see* **Note 7**).

2.2 Microscope

1. A confocal laser scanning microscope. Here, a Leica SP5 equipped with an HCX PL APO lambda blue 63.0 × 1.40 OIL UV objective is used.
2. Lasers for excitation at 488 nm, 561 nm and 633 nm.
3. Optional: Excitation/emission filter sets (e.g., Leica TX2 (*see* **Note 8**).
4. A chamber for incubation at 37 °C/5% CO_2 that can be protected from light. A microscope incubator box and control device from EMBLEM Technology Transfer GmbH, Germany is used in our work.

2.3 Software

1. LAS AF microscopy software (Leica).
2. Fiji distribution [13] of ImageJ [14], version 2.0.0.
3. R, version 3.5.2.
4. R package *EBImage*, version 4.24.0 [15].
5. R package *nlme*, version 3.1–137 [16].

Fig. 2 (continued) recruitment. iR713, iRFP713; mCh, mCherry. (**c**) Representative confocal laser scanning microscopy images for reversibly recruiting an mCherry-labeled mock effector (PHR-mCherry-NLS). The array location is marked by CIBN-TetR-iRFP713 (right, top). Prior to light induction, PHR-mCherry-NLS is evenly distributed throughout the cell (left, top). Upon illumination at 488 nm, it accumulates at the array within seconds (middle). After recruitment, it dissociates again in the absence of blue light (left, bottom) within 10-20 min. Notably, the iRFP713-tagged localizer construct can be detected continuously (right, bottom). The time points for the localizer constructs (right, bottom) are the same as for the effector (left, bottom). Note that iRFP713 is susceptible to photobleaching (*see* **Note 1**). Image intensities have been adjusted nonlinearly (gamma transformation) to improve the visibility. Scale bars: 5 μm; insets: 2× magnification

3 Methods

The protocols provided here were applied to the characterization of reversible association to and dissociation from a gene array in a reporter cell line (Fig. 2b). The use of iRFP713 and mCherry in these assays can be easily adapted for tagging other loci (telomeres, nucleoli, nuclear lamina, PML bodies, etc.) or readouts (e.g., MS2 coat protein to detect RNA carrying MS2 loop sequences) [11].

3.1 Cell Culture

U2OS 2-6-3 cells are cultured at 37 °C in 5% CO_2. They should be passaged every 3–4 days and can be frozen in DMEM containing 10% DMSO and 40% FBS.

1. Seed U2OS 2-6-3 cells in a dish that is compatible with live cell microscopy (e.g., Lab-Tek slides). To this end, passage the cells according to standard cell culture protocols. They should be 50–90% confluent on the next day for transfection.
2. On the next day, transfect cells with a localizer and an effector construct (e.g., CIBN-TetR-iRFP713 and PHR-mCherry-VP16 or -NLS) according to the manufacturer's protocol (*see* **Note 9**). Take care to protect transfected cells from light by placing them in a nontransparent Styrofoam box and by minimizing handling. It is recommended to transfect two wells and use one for searching the right focal plane using the ocular and one for the actual measurements.

3.2 Microscopy

The microscopy part of the experiment can be carried out 18–48 h after transfection for the constructs described here. Shorter transfection times might lead to incomplete maturation of the constructs whereas dilution or loss of the constructs will increase at longer transfection times. The imaging parameters given here provide reasonable time resolution for rapid recruitment and sufficient spatial resolution to reliably locate the array. Depending on the application and the used constructs, the temporal and spatial resolution should be adjusted. We have recorded high-resolution images before and after recruitment and after the reversibility series to be able to assess the amount of prerecruitment and residual enrichment of the effector construct at the array. All multicolor images are recorded using the "between lines" sequential scan modus to ensure that the images from the different scans are aligned.

1. Preheat the incubation chamber about 1 h prior to imaging to ensure that the microscope optics are at a constant temperature, thereby limiting drifting during the acquisition.
2. Place the cells on the microscope using the red flashlight. During the transfer, switch off all other (blue/white) light sources including computer screens.

3. Search for transfected cells using the ocular and an appropriate filter cube (e.g., Leica TX2 or Y5, *see* **Note 8**).
4. Set up sequential imaging in the LAS AF software with two scans. Use the following excitation/emission parameters (Fig. 1b): scan #1 (iRFP713), excitation at 633 nm, emission detection at 645–800 nm; scan #2 (mCherry), excitation at 561 nm, emission detection at 575–620 nm.
5. Use laser excitation and PMT detection in the microscope software to find a transfected cell (*see* **Note 10**). This should be done in a well that has not been used to initially search for transfected cells (in **step 3**) to minimize premature light exposure for the cell of interest.
6. Zoom in (e.g., zoom factor 9 corresponding to 53.5 nm per pixel) and adjust the excitation intensities, so that no pixels are saturated (*see* **Note 11**). Use the localizer channel (i.e., scan #1, iRFP713) to make sure that the array is in focus.
7. Record prerecruitment images (*see* **Note 12**). High quality: 512×512 px, 400 Hz line scan frequency, 4× line average (Fig. 2c). Low quality (optional): 256×256 px, 1400 Hz line scan frequency, 1× line average.
8. Exclude scan #1 and switch on the 488 nm laser (in addition to the 561 nm laser) in scan #2. Record a recruitment series with the same low-quality parameters as in **step 7** (*see* **Note 13**, Fig. 2c). The frame time should be minimized (204 ms for the abovementioned imaging parameters).
9. Switch off the 488 nm laser in scan #2 and include scan #1 (iRFP713).
10. Optional: Record a high-quality image (parameters as listed in **step 7**) immediately after the recruitment.
11. Reduce the line average to 1× to limit photobleaching and record a dissociation series of both channels (90 frames, 15 s frame time, 512×512 px, 400 Hz line scan frequency, *see* **Note 14**, Fig. 2c).
12. Optional: Record a high-quality image with the parameters listed in **step 7** (end-point).
13. Move on to the next cell and repeat **steps 5** through **12**.

3.3 Recruitment Analysis

The analyses of the recruitment time series were carried out essentially as described previously [10] (*see* Table 1). Image analysis was done in ImageJ and additional analyses were done using R.

1. Load the recruitment stack into ImageJ.
2. Make a maximum intensity projection of the time series stack (*Image* → *Stacks* → *Z Project...*). This projection serves to determine the area that is occupied by the array over the entire time course.

Table 1
BLInCR association and dissociation kinetics determined with different fluorophores or imaging settings

Experiment	Effector	Localizer[a]	*z*-axis image[b]	Data fit approach[c]	Characteristic time[d]
Association	PHR-mCherry-VP16	CIBN-TetR-iRFP713	Single	Individual	8.2 ± 6.1 s
				Global	8.0 ± 5.3 s
	PHR-YFP-VP16 [e]	CIBN-TetR-tagRFP-T	Single	Individual	11.9 ± 5.6 s
				Global	10.9 ± 3.5 s
	PHR-mCherry-NLS	CIBN-TetR-iRFP713	Single	Individual	8.6 ± 4.0 s
				Global	9.2 ± 3.9 s
	PHR-YFP-NLS [e]	CIBN-TetR-tagRFP-T	Single	Individual	25.9 ± 12.3 s
				Global	19.4 ± 3.2 s
Dissociation	PHR-mCherry-VP16	CIBN-TetR-iRFP713	Single	Individual	4.4 ± 0.8 min
	PHR-mCherry-VP16[f]	CIBN-TetR	Stack	Individual	4.9 ± 0.8 min
	PHR-mCherry-NLS	CIBN-TetR-iRFP713	Single	Individual	5.1 ± 0.5 min
	PHR-mCherry-NLS [f]	CIBN-TetR	Stack	Individual	4.8 ± 0.6 min

[a]To reliably localize the reporter array either a fluorescently labeled CIBN-LacIR or CIBN-LacI construct can be used
[b]Kinetics were recorded either by imaging one optical section ("single") or by recording image stacks (typically 4-6 optical sections, spaced 0.4–0.5 μm apart)
[c]For the individual fit procedure, all parameters in the fit equation given in **step 10** were determined for each single cell. For the global fit procedure, the rates k_1 and k_2 were fitted globally considering all cells from all association experiments listed here ($n = 61$). This assumes that the underlying rate processes, which recapitulate PHR photoswitching as well as PHR-CIBN and PHR-PHR association, are identical for the different constructs. The plateau value a as well as the contributions of the different rate processes to the overall binding kinetics b and c were fitted individually for each cell also in the global fit procedure
[d]The characteristic time refers to the time at which 50% of the effector has associated to ($\tau_{1/2}$) or dissociated from ($t_{1/2}$) the localizer protein bound to the array. The mean and standard deviation ($n > 10$ for all cases) is displayed
[e]Data from ref. [10] were analyzed to retrieve averaged results from individual fits. The global fit results differ slightly from the previously published data since they were analyzed with the new data from recruitment to CIBN-TetR-iRFP713 described here
[f]Values reported previously in ref. [10]

3. Select a circular region around the array and add the selection to the ROI manager (*Analyze* → *Tools* → *ROI Manager*...).
4. Optional: create a mask from the selection and save it for documentation purposes (*Edit* → *Selection* → *Create Mask*).
5. Repeat **steps 3** and **4** for a nuclear reference (*see* **Note 15**) and background region (Fig. 3a).
6. Select the recruitment series, then select the three ROIs in the ROI manager and measure their mean fluorescence intensity (*ROI Manager* → *More* >> → *Multi Measure*, Fig. 3a).
7. Save the data and load it into R.
8. Subtract the mean background intensity $I_{back}(t)$ from the mean intensity of the nuclear reference region $I_{nuc}(t)$ and fit the resulting (decaying) background-corrected reference intensity

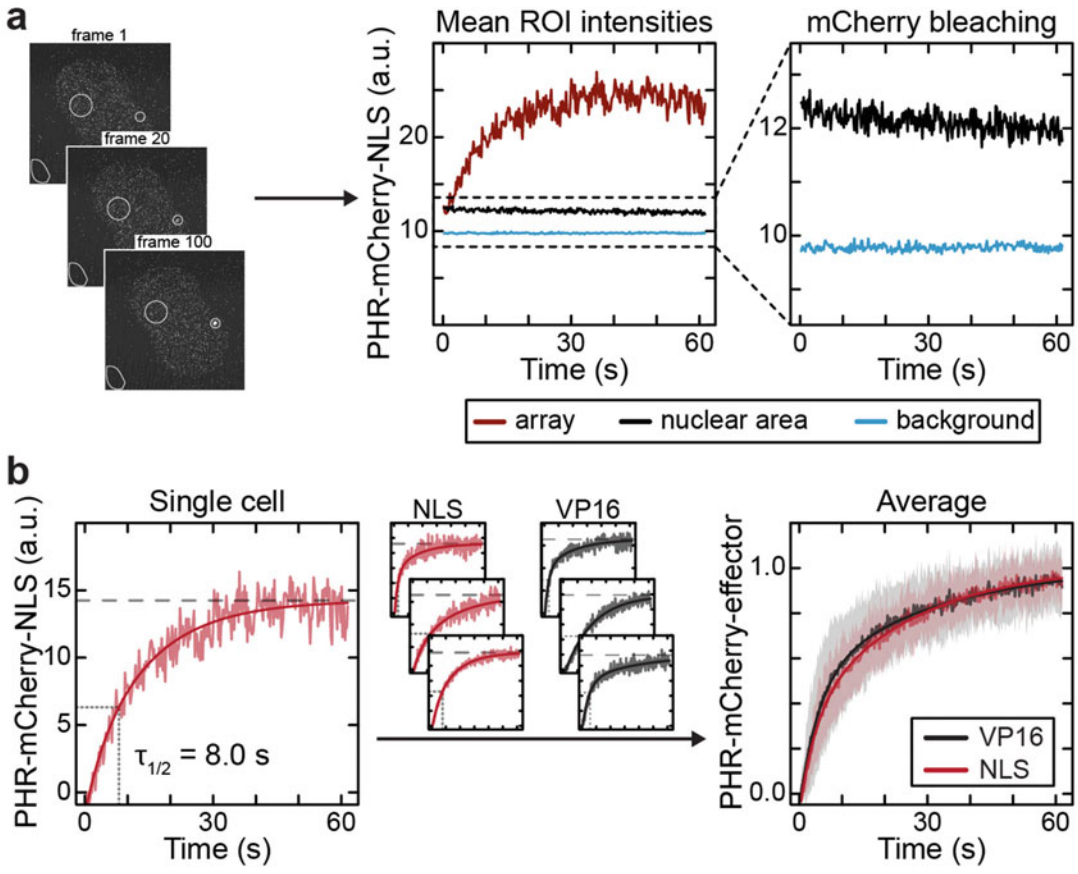

Fig. 3 Measuring BLInCR association kinetics. (**a**) Quantification of images. Regions of interest (ROIs) for array, nuclear reference region and background were selected manually on a maximum intensity projection of the 300 recruitment frames. Mean intensities in the three ROIs are measured for each frame (left), yielding the mean intensity traces (center). Photobleaching of mCherry was estimated from the nuclear area and the background mean intensity traces (right). (**b**) Data analysis. Single bleach- and nuclear background-corrected array intensities (left) are fitted to a model assuming two parallel first-order reactions (*see* **Note 17**). Measurements of several cells are normalized to account for different transfection efficiencies and averaged (right) to be able to compare the recruitment kinetics of different effectors. The average and standard deviations of VP16 ($n = 12$) and the mock effector NLS ($n = 12$) as well as the respective fits of the average curves are displayed. The times to reach half-maximal intensities are listed in Table 1

$I_{\mathrm{ref}}(t) = I_{\mathrm{nuc}}(t) - I_{\mathrm{back}}(t)$ with a single exponential to estimate mCherry bleaching (*see* **Note 16**, Fig. 3a): $I_{\mathrm{ref}}(t) = a_{\mathrm{ref}} \cdot \exp(-k_{\mathrm{bleach}} \cdot t)$, for example, by using the *nls* function from the *nlme* package in R.

9. Subtract the mean intensity of the reference region $I_{\mathrm{nuc}}(t)$ from the mean intensity of the array $I_{\mathrm{array}}(t)$ and correct the resulting net array signal $I(t) = I_{\mathrm{array}}(t) - I_{\mathrm{nuc}}(t)$ for bleaching using the estimated bleach parameter from **step 8**: $E(t) = I(t)/\exp(-k_{\mathrm{bleach}} \cdot t)$.

10. Fit the bleach-corrected effector enrichment at the array $E(t)$ (Fig. 3b, left) with a double exponential $E(t) = a - b \cdot \exp(-k_1 \cdot t) - c \cdot \exp(-k_2 \cdot t)$ (*see* **Note 17**), for example, using the *nls* function from the *nlme* package in R.
11. Retrieve the characteristic time to reach half-maximal levels $\tau_{1/2}$ from the model in **step 10** and the half-maximal level $E(\tau_{1/2})$ (*see* **Note 18**) by solving $0 = b\ (1 - 2 \cdot \exp(-k_1 \cdot \tau_{1/2})) + c\ (1 - 2 \cdot \exp(-k_2 \cdot \tau_{1/2}))$, for example, using the *uniroot* function in R.
12. Optional: Normalize the enrichment $E(t)$ to the plateau value a to account for different transfection efficiencies: $E_{\mathrm{norm}}(t) = E(t)/a$. The traces that are normalized in this way can be used to calculate an average enrichment curve as shown in Fig. 3b (right).
13. Repeat **steps 1** through **12** for all cells.
14. Remove cells that moved during image acquisition or had a very low signal-to-noise ratio.

3.4 Reversibility Analysis

While the light-induced association reaches a plateau within a minute (Fig. 3), the analysis of the dissociation kinetics requires image acquisition on a time scale that is at least an order of magnitude larger (Table 1). During this longer acquisition time period, cells frequently undergo considerable movements and deformation that need to be accounted for in the analysis. Hence, nuclei and array regions were selected semiautomatically in each time frame based on intensity thresholds. The R package *EBImage* was used for this purpose. Alternatively, this task can also be accomplished with ImageJ (*Image* → *Adjust* → *Threshold*...).

1. Concatenate a (high-quality) prerecruitment image with the reversibility series (e.g., using ImageJ: *Image* → *Stacks* → *Tools* → *Concatenate*...).
2. Load the image series into R using the *EBImage* package. Alternatively, load the image series into ImageJ.
3. Use the PHR-mCherry-effector channel to segment the nuclei in each frame of the time series (*see* **Note 19**, Fig. 4a).
4. Use the CIBN-iRFP713-localizer channel to segment the array in each frame of the time series (*see* **Note 20**, Fig. 4a).
5. Create a mask of the nucleus without the array by subtracting the array mask from the whole nucleus mask. This selection will be referred to as "nucleus" subsequently.
6. Measure the mean fluorescence intensity in the respective selections for each time point (Fig. 4a).
7. Optional: Load the intensity data into R if ImageJ was used for segmentation.

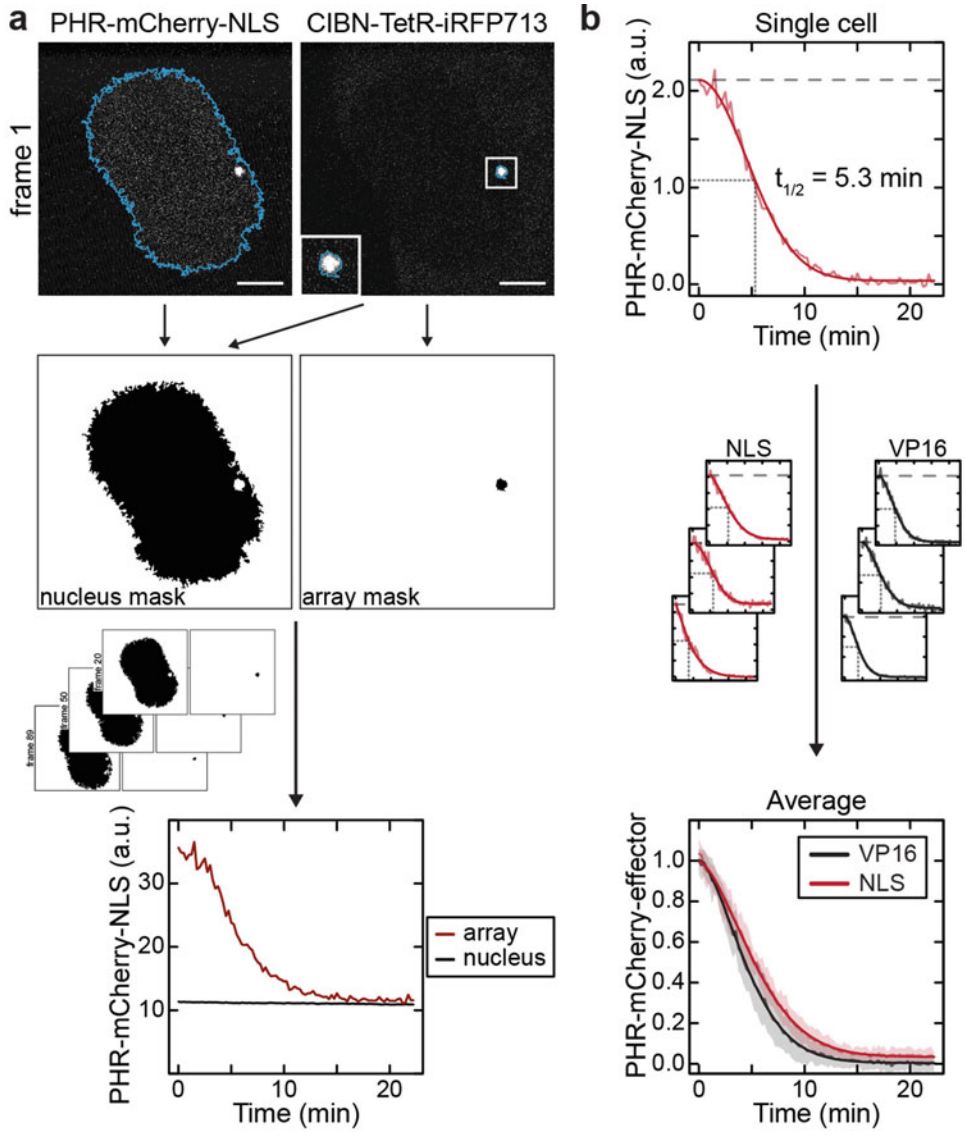

Fig. 4 Measuring BLInCR dissociation kinetics. (**a**) Quantification of images. The nucleus and array ROI were segmented based on intensity thresholds in the PHR-mCherry-NLS and the CIBN-TetR-iRFP713 image, respectively (top). The array mask was subtracted from the nucleus mask to yield the nucleus without array (middle). The masks were created for each frame and their mean fluorescence intensity was measured (bottom). Scale bars, 5 μm. (**b**) Data analysis. Bleach-, and nuclear background-corrected array intensities are corrected for the initial prerecruitment value (*see* **Note 22**) for individual cells and fitted to an exponential decay with a time-dependent (i.e., concentration-dependent) rate similar to the model described in ref. [17] (top). Multiple measurements are normalized to account for different effector expression and averaged to compare the recruitment kinetics of different effectors (bottom). The average and standard deviations of VP16 ($n = 11$) and the mock effector NLS ($n = 12$) are displayed. The resulting half-life times $t_{1/2}$ are listed in Table 1

8. Calculate the enrichment of fluorescence intensity at the array E_{array} from the array intensity $I_{\text{array}}(t)$ and the nucleus intensity (array excluded) $I_{\text{nucleus}}(t)$ and correct it for bleaching (*see* **Note 21**): $E_{\text{array}}(t) = (I_{\text{array}}(t) - I_{\text{nucleus}}(t))/I_{\text{nucleus}}(t)$.
9. Subtract the array enrichment of the "pre" image recorded before the initial recruitment from the array enrichment (*see* **Note 22**): $E(t) = E_{\text{array}}(t) - E_{\text{array}}(\text{"pre"})$.
10. Fit the corrected array enrichment $E(t)$ (Fig. 4b, top), for example using the *nls* function from the *nlme* package in R. A single exponential with a time-dependent (i.e., concentration-dependent) rate can be used $E(t) = a \cdot \exp(-k \cdot t^m) + c$ [17]. For alternative models *see* **Note 23**.
11. Determine the characteristic half-life $t_{1/2}$ from the model in **step 10** and the half-maximal level $E(t_{1/2})$ (*see* **Note 18**) by solving $0 = 2 \cdot \exp(-k \cdot {t_{1/2}}^m) - 1$, for example, using the *uniroot* function in R.
12. Optional: Normalize the cells to their respective initial levels ($E_{\text{norm}}(t) = E(t)/(a + c)$) to calculate an average curve as in Fig. 4b.

4 Notes

1. The main limitation of using iRFP713 for BLInCR applications is its relatively low brightness and high susceptibility to photobleaching. This is less of an issue for tracing the reporter array used here, which has a high number of fluorophore binding sites. However, for other applications where detection sensitivity is crucial, for example, for tracing RNA production, iRFP713 is not well-suited. Since the development and improvement of autofluorescent proteins with near-infrared emission is currently an active research area [8], we anticipate that brighter and more photostable constructs will become available. Recently, iRFP670 (λ_{ex} = 643 nm, λ_{em} = 670 nm) [18] and miRFP670nano (λ_{ex} = 645 nm, λ_{em} = 670 nm) [19] have been introduced but we have not tested them yet. We expect them to be applicable for BLInCR reversibility experiments with the protocol used here when adjusting for their somewhat different spectral properties.
2. In principle, any cell type that expresses the tagged protein constructs needed is suitable for BLInCR. We have chosen U2OS 2-6-3 for its transcription reporter, its easily detectable single array and its high transfection efficiency.

3. Alternatively, 10-well CELLview slides (Greiner Bio-One GmbH, Germany) can be used, which have black walls between the wells to limit stray light from imaging in a neighboring well. However, we did not observe a difference as compared to the transparent walls of the Lab-Tek slides, in particular when using laser excitation for imaging. In contrast, observing cells through the ocular with a mercury vapor lamp causes more stray light, which can cause premature photoswitching (depending on the filter sets and light intensities used).
4. To limit premature light exposure, it is advantageous to use a transfection reagent that does not need to be removed from the medium before imaging. We have also used lipofectamine 3000 for immortalized mouse embryonic fibroblasts (iMEFs) without changing the medium after transfection.
5. The localizer construct used here binds to *tet*O in the absence of doxycycline. We used doxycycline-free medium, resulting in high-affinity binding of CIBN-TetR-iRFP713 as soon as the construct was expressed. This caused no problems for transient transfections (24–48 h), but cells should be grown in doxycycline-containing medium for long-term experiments or when generating stable cell lines. Using reverse TetR [20], which binds *tetO* in the presence of doxycycline, is also a recommended option for the latter types of experiments (also *see* ref. [21] for a review on TetR properties and variants).
6. Other suitable constructs are also available: CIBN-TetR-tagRFP-T (localizer, Addgene #103809), PHR-iRFP713-VP16 (effector, Addgene #103823), PHR-iRFP713 (mock effector, Addgene #103818). For other effectors and localizers see the Addgene entries associated with [10].
7. To avoid premature light-induced binding of effectors, transfected cells should be kept in the dark at all times. White Styrofoam boxes are not suited for this purpose since they do transmit some light. If cells need to be handled after transfection, switch off all white light sources and use a red safelight (e.g., a removable bike tail light).
8. The Leica TX2 filter cube can be helpful to initially localize cells. It limits the excitation light using a bandpass filter (BP 560/40). Since it can also cause effector recruitment at high light intensities, it is recommended to only use the ocular to adjust the focal plane in the very beginning of the experiment. This can also be done in a well that is not used for the actual measurements later. Other filter cubes such as the Leica Y5 should work well but we have not tested them.
9. We have adapted the Xtreme Gene 9 (Roche, Germany) protocol for use in 8-well Lab-Tek slides as follows (amounts for transfecting one well corresponding to 0.8 cm^2): add 0.8 µl Xtreme Gene 9 reagent to 20 µl Opti-MEM in a suitable

reaction tube (e.g., 1.5 ml Eppendorf), add 300–400 ng plasmid DNA at a 1:1 ratio of localizer and effector constructs, flick the tube for mixing and incubate the mixture for 15 min at room temperature before adding the mix to the medium.

10. It is recommended to use cells that express the respective constructs at low levels. In our experience, high expression levels of PHR constructs lead to significant prerecruitment in the absence of light.
11. Keep in mind that the effector intensity at the array will be high upon recruitment. The intensity in the image prior to recruitment should thus be rather low to avoid oversaturated pixels at the array after recruitment. In addition, do not change the excitation during imaging to obtain comparable results.
12. The high-quality image is well-suited to ensure that there is no prerecruitment of PHR-mCherry-effector. It is also used in the analysis of the reversibility series (*see* Subheading 3.4). The low-quality image is recorded with the same imaging parameters as the recruitment series and can thus be used to assess the laser intensities. However, it cannot be included in the quantitative analyses of the recruitment series because the 488 nm laser is used for the recruitment but switched off during imaging prior to recruitment. Since mCherry has some absorbance at 488 nm (Fig. 1a), the absolute intensities of prerecruitment and recruitment images are not comparable.
13. For recruitment, the localizer was not imaged in order to increase the temporal resolution. We have recorded 300 frames corresponding to ~1 min total imaging time, during which the cells generally did not move or drift excessively. This time was generally sufficient to reach a plateau of PHR-mCherry-effector intensity at the array. The PHR switching and thus the recruitment kinetics also depend on the intensity of the blue light used. It should therefore be kept constant for all experiments to ensure comparability.
14. For the reversibility series, both localizer and effector images were recorded because the cells move, deform, and/or drift significantly over the recording time of 22.5 min. Hence, it is advantageous to record the localizer image to ensure that the array is still in focus. This is different from the approach used in our previous work [10] where image stacks were recorded to ensure that all signal from the array was detected without visualizing the array over time.
15. Here, we have used a nuclear reference region as opposed to the entire nucleus, because the fluorescently tagged (mock) effectors have a preference to be enriched or depleted from nucleoli. The mCherry-tagged effectors used here tend to be depleted from nucleoli. Hence, the mean intensity of the

nucleus will always be smaller than that of the array even if no effector is recruited. The nuclear reference region was placed in a region that had homogeneously distributed mCherry signal similar to that of the array; hence, $E(0) \approx 0$ if no construct is recruited without further normalization. Using a ring-shaped reference region around the array selection would also be feasible but is impractical since the array is often located close to the nuclear lamina.

16. We have fitted the data with a single exponential for practical reasons without any assumptions about the bleach process. For different time scales, a different model might be more appropriate. The background-corrected reference intensity I_{ref} can be fitted with any function that describes the data well and yields a constant value for the bleach-corrected reference intensity, which was in our case $I_{\mathrm{ref,cor}} = (I_{\mathrm{nuc}} - I_{\mathrm{back}})/\exp(-k_{\mathrm{bleach}} \cdot t) = a_{\mathrm{ref}}$. Alternatively, the net array intensity $I(t) = I_{\mathrm{array}}(t) - I_{\mathrm{nuc}}(t)$ can simply be divided by the intensity of the nuclear reference region I_{nuc} yielding $E(t) = I(t)/I_{\mathrm{nuc}}(t)$. The latter approach was used for the longer dissociation time series (Subheading 3.4). Using a (smooth) fit function for bleach correction was advantageous for the rather noisy association curves.

17. The fit model considers two parallel first-order reactions for binding to two subpopulations of binding sites. The two resulting rates could correspond to PHR photoswitching followed by (1) PHR-CIBN heterodimerization and by (2) PHR-PHR oligomerization and optodroplet formation [22, 23]. Note that the resulting times to reach half-maximal levels are shorter for the PHR-mCherry-effector constructs used here compared to the PHR-YFP-effector constructs used previously [10] (Table 1). This could be due to different propensities of the mCherry and YFP constructs to allow PHR-PHR oligomerization and optodroplet formation. A certain heterogeneity of binding kinetics between cells transfected with the same constructs is expected because the binding reaction rate depends on the (variable) expression level of the PHR ligand.

18. The half-maximal levels $E(\tau_{1/2})$ for the association and $E(t_{1/2})$ for the dissociation were calculated from the respective initial enrichment $E(0)$ and the respective plateau value $E(\infty)$ as $E(\tau_{1/2}) = E(0) + (E(\infty) - E(0))/2$ and, analogously, $E(t_{1/2}) = E(0) + (E(\infty) - E(0))/2$.

19. We have used the Otsu method [24] to determine a threshold and multiplied it with a factor of typically 0.7 (0.6–0.9). This factor was determined separately for each cell and was necessary because of different cytoplasmic or background signals.

The otsu() function in R calculates the threshold for each image in an image series. However, this histogram-based algorithm occasionally recognizes the cell as background and large arrays (compared to the cell size) as foreground resulting in poor segmentation of some of the nuclei in a series. Hence, we have determined the threshold on the last image of the effector series (where the effector construct has dissociated from the array) and used this value for segmenting the entire stack.

20. The threshold selection for the array segmentation was done as for the nucleus segmentation (*see* **Note 19**), but the factor with which the Otsu threshold was multiplied was typically 3.0 (2.5–5.0).
21. For the bleach correction of the dissociation curves, we have used the mean nucleus fluorescence intensity assuming that it bleaches in the same manner as the array intensity.
22. This normalization step is necessary because $E_{\text{array}}(0) \neq 0$ even if no construct is recruited (for an explanation, *see* **Note 15**).
23. The model in **step 10** described our data well (Fig. 4b), but alternative models can be used to describe the dissociation kinetics and interpret the fitted parameters. One model is represented by $E(t) = a \cdot \exp(-k \cdot t)/(b + \exp(-k \cdot t)) + c$. Here, b is a parameter related to the dissociation constant and concentration of binding-competent PHR molecules at the start of the dissociation time course. The parameter c accounts for a residual basal intensity level after dissociation. This equation is derived from the analytical solution to a model, in which a ligand can switch between a binding-competent and a noncompetent conformation with rate k. In the dark, the binding competent state B decays according to $B(t) = B_0 \cdot \exp(-k \cdot t)$. The binding to the target site S is assumed to be significantly faster than the conformational switch. Thus, at any time the concentration of the chromatin bound complex $BS(\mathrm{t})$ is in equilibrium: $BS(t) = S_{\text{total}} \cdot B(t)/(B(t) + k_{\text{off}}/k_{\text{on}})$ leading to $b = K_{\text{d}}/B_0$ and $a = S_{\text{total}}$ where $K_{\text{d}} = k_{\text{off}}/k_{\text{on}}$ is the dissociation constant. With this approach the conformational reversion rate k is obtained while a and b cannot be interpreted without knowledge about the relation of fluorescence intensity and absolute concentrations. Another possibility to represent the dissociation process would be to use a model with two sequential reactions with rate k according to $B_0\,(1 + k \cdot t) \cdot \exp(-k \cdot t) + c$ (*see* ref. [10] for the use of sequential reaction schemes to fit the transcription activation process).

Acknowledgments

We thank the DKFZ light microscopy core facility for technical support for imaging. This work was supported by the Deutsche Forschungsgemeinschaft (DFG grant RI 1283/14-1 to K.R.).

References

1. Losi A, Gardner KH, Moglich A (2018) Blue-light receptors for optogenetics. Chem Rev 118(21):10659–10709. https://doi.org/10.1021/acs.chemrev.8b00163
2. Liu H, Yu X, Li K, Klejnot J, Yang H, Lisiero D, Lin C (2008) Photoexcited CRY2 interacts with CIB1 to regulate transcription and floral initiation in Arabidopsis. Science 322(5907):1535–1539. https://doi.org/10.1126/science.1163927
3. Kennedy MJ, Hughes RM, Peteya LA, Schwartz JW, Ehlers MD, Tucker CL (2010) Rapid blue-light-mediated induction of protein interactions in living cells. Nat Methods 7 (12):973–975. https://doi.org/10.1038/nmeth.1524
4. Salomon M, Christie JM, Knieb E, Lempert U, Briggs WR (2000) Photochemical and mutational analysis of the FMN-binding domains of the plant blue light receptor, phototropin. Biochemistry 39(31):9401–9410. https://doi.org/10.1021/bi000585+
5. Huala E, Oeller PW, Liscum E, Han IS, Larsen E, Briggs WR (1997) Arabidopsis NPH1: a protein kinase with a putative redox-sensing domain. Science 278 (5346):2120–2123. https://doi.org/10.1126/science.278.5346.2120
6. Niopek D, Benzinger D, Roensch J, Draebing T, Wehler P, Eils R, Di Ventura B (2014) Engineering light-inducible nuclear localization signals for precise spatiotemporal control of protein dynamics in living cells. Nat Commun 5:4404. https://doi.org/10.1038/ncomms5404
7. Shaner NC, Campbell RE, Steinbach PA, Giepmans BN, Palmer AE, Tsien RY (2004) Improved monomeric red, orange and yellow fluorescent proteins derived from Discosoma sp. red fluorescent protein. Nat Biotechnol 22 (12):1567–1572. https://doi.org/10.1038/nbt1037
8. Karasev MM, Stepanenko OV, Rumyantsev KA, Turoverov KK, Verkhusha VV (2019) Near-infrared fluorescent proteins and their applications. Biochemistry (Mosc) 84(Suppl 1):S32–S50. https://doi.org/10.1134/S0006297919140037
9. Filonov GS, Piatkevich KD, Ting LM, Zhang J, Kim K, Verkhusha VV (2011) Bright and stable near-infrared fluorescent protein for in vivo imaging. Nat Biotechnol 29(8):757–761. https://doi.org/10.1038/nbt.1918
10. Rademacher A, Erdel F, Trojanowski J, Schumacher S, Rippe K (2017) Real-time observation of light-controlled transcription in living cells. J Cell Sci 130(24):4213–4224. https://doi.org/10.1242/jcs.205534
11. Trojanowski J, Rademacher A, Erdel F, Rippe K (2019) Light-induced transcription activation for time-lapse microscopy experiments in living cells. In: Shav-Tal Y (ed) Imaging gene expression: methods and protocols, methods in molecular biology, vol 2028. Springer Nature, New York, pp 251–270. https://doi.org/10.1007/978-1-4939-9674-2_17
12. Janicki SM, Tsukamoto T, Salghetti SE, Tansey WP, Sachidanandam R, Prasanth KV, Ried T, Shav-Tal Y, Bertrand E, Singer RH, Spector DL (2004) From silencing to gene expression: real-time analysis in single cells. Cell 116 (5):683–698. https://doi.org/10.1016/s0092-8674(04)00171-0
13. Schindelin J, Arganda-Carreras I, Frise E, Kaynig V, Longair M, Pietzsch T, Preibisch S, Rueden C, Saalfeld S, Schmid B, Tinevez JY, White DJ, Hartenstein V, Eliceiri K, Tomancak P, Cardona A (2012) Fiji: an open-source platform for biological-image analysis. Nat Methods 9(7):676–682. https://doi.org/10.1038/nmeth.2019
14. Schneider CA, Rasband WS, Eliceiri KW (2012) NIH image to ImageJ: 25 years of image analysis. Nat Methods 9(7):671–675
15. Pau G, Fuchs F, Sklyar O, Boutros M, Huber W (2010) EBImage—an R package for image processing with applications to cellular phenotypes. Bioinformatics 26(7):979–981. https://doi.org/10.1093/bioinformatics/btq046
16. Pinheiro J, Bates D, DebRoy S, Sarkar D, R_Core_Team (2018) nlme: linear and nonlinear mixed effects models. R package version 3. 1-137.https://CRAN.R-project.org/package=nlme
17. Sing CE, Olvera de la Cruz M, Marko JF (2014) Multiple-binding-site mechanism

explains concentration-dependent unbinding rates of DNA-binding proteins. Nucleic Acids Res 42(6):3783–3791. https://doi.org/10.1093/nar/gkt1327

18. Shcherbakova DM, Verkhusha VV (2013) Near-infrared fluorescent proteins for multicolor in vivo imaging. Nat Methods 10 (8):751–754. https://doi.org/10.1038/nmeth.2521
19. Oliinyk OS, Shemetov AA, Pletnev S, Shcherbakova DM, Verkhusha VV (2019) Smallest near-infrared fluorescent protein evolved from cyanobacteriochrome as versatile tag for spectral multiplexing. Nat Commun 10(1):279. https://doi.org/10.1038/s41467-018-08050-8
20. Gossen M, Freundlieb S, Bender G, Muller G, Hillen W, Bujard H (1995) Transcriptional activation by tetracyclines in mammalian cells. Science 268(5218):1766–1769. https://doi.org/10.1126/science.7792603
21. Berens C, Hillen W (2003) Gene regulation by tetracyclines. Constraints of resistance regulation in bacteria shape TetR for application in eukaryotes. Eur J Biochem 270 (15):3109–3121. https://doi.org/10.1046/j.1432-1033.2003.03694.x
22. Bugaj LJ, Choksi AT, Mesuda CK, Kane RS, Schaffer DV (2013) Optogenetic protein clustering and signaling activation in mammalian cells. Nat Methods 10(3):249–252. https://doi.org/10.1038/nmeth.2360
23. Shin Y, Berry J, Pannucci N, Haataja MP, Toettcher JE, Brangwynne CP (2017) Spatiotemporal control of intracellular phase transitions using light-activated optoDroplets. Cell 168(1-2):159–171.e114. https://doi.org/10.1016/j.cell.2016.11.054
24. Otsu N (1979) A threshold selection method from gray-level histograms. IEEE Trans Sys Man Cyber 9(1):62–66. https://doi.org/10.1109/tsmc.1979.4310076